Compact electrically detected magnetic resonance setup

Michael Eckardt, Jan Behrends, Detlef Münter, and Wolfgang Harneit

Compact electrically detected magnetic resonance setup

Michael Eckardt,[1,a] Jan Behrends,[2] Detlef Münter,[3] and Wolfgang Harneit[1,b]

[1]*Institute of Physical Chemistry, Johannes Gutenberg University Mainz, Duesbergweg 10-14, 55099 Mainz, Germany*
[2]*Berlin Joint EPR Lab, Fachbereich Physik, Freie Universität Berlin, Arnimallee 14, 14195 Berlin, Germany*
[3]*Magnettech GmbH, Louis-Blériot-Str. 5, 12487 Berlin, Germany*

Electrically detected magnetic resonance (EDMR) is a commonly used technique for the study of spin-dependent transport processes in semiconductor materials and electro-optical devices. Here, we present the design and implementation of a compact setup to measure EDMR, which is based on a commercially available benchtop electron paramagnetic resonance (EPR) spectrometer. The electrical detection part uses mostly off-the-shelf electrical components and is thus highly customizable. We present a characterization and calibration procedure for the instrument that allowed us to quantitatively reproduce results obtained on a silicon-based reference sample with a "large-scale" state-of-the-art instrument. This shows that EDMR can be used in novel contexts relevant for semiconductor device fabrication like clean room environments and even glove boxes. As an application example, we present data on a class of environment-sensitive objects new to EDMR, semiconducting organic microcrystals, and discuss similarities and differences to data obtained for thin-film devices of the same molecule. © 2015 Author(s). All article content, except where otherwise noted, is licensed under a Creative Commons Attribution 3.0 Unported License. [http://dx.doi.org/10.1063/1.4919247]

I. INTRODUCTION

Electrically detected magnetic resonance (EDMR) has proven to be a powerful tool for investigating the influence of paramagnetic states on electronic transport and recombination phenomena in semiconductor materials and electronic devices.[1–6] In contrast to electron paramagnetic resonance (EPR) where any kind of unpaired electron can in principle lead to a signal, EDMR is only sensitive to those spins involved in spin-dependent processes that affect the lifetimes and transport of elementary excitations. The corresponding selection rules can be quite strict even at room temperature, especially in organic materials, where they lead to relatively long-lived spin pair states. Pair partners may be photo-excited electrons and holes that preferably recombine when they are in a singlet pair state, or like charges that contribute to a spin-dependent current. Spin pairs that give rise to an EDMR signal can be found at deep levels due to the disorder in amorphous parts of a device as well as at grain boundaries between different crystalline parts or at contact interfaces of materials. Therefore, EDMR is the method of choice for the elucidation of mechanisms limiting the performance of electro-optical devices such as silicon-based as well as organic solar cells and light emitting diodes.

Here, we focus on the design and operation of a compact EDMR spectrometer, which can be used to characterize complete electronic devices under operating conditions like room temperature and white-light illumination. Being very compact, our setup also allows for the investigation of organic semiconductors without the need for encapsulation, by moving the setup into the protective atmosphere of a glove box. This simplifies the elucidation of mechanisms limiting the performance

---

[a]michael.eckardt@uni-mainz.de
[b]harneit@uni-mainz.de

of these devices right after their production, including those due to encapsulation procedures. The results presented in this publication where obtained using a thin-film solar cell made of hydrogenated microcrystalline silicon (μc-Si:H) in a p-i-n configuration as a well-defined reference sample, and on C_{60} microwires as a new class of samples accessible with this spectrometer.

II. THE EDMR SETUP

To induce an EPR transition in a spin $S = 1/2$ system, the sample has to be placed inside an external magnetic field B_0 leading to a Zeemann splitting of the two spin states with $m_S = \pm 1/2$. The energy difference is then $\Delta E = g\mu_B B_0$, where g denotes the characteristic g-factor of the investigated paramagnetic state, and μ_B the Bohr magneton.[7] Applying a microwave magnetic field, $B_1 \propto \cos(2\pi \nu t)$, perpendicular to B_0, the transition can take place if the microwave frequency $\nu = g\mu_B B_0/h$, with h being Planck's constant. In contrast to EPR, where the cavity-reflected microwave power gives rise to the detected signal, EDMR uses an electrical detection scheme to measure the spin-dependent currents. Since electric currents can be detected with very high accuracy, the electrical detection concept also leads to an increase in sensitivity over conventional EPR spectroscopy.[2] Figure 1 illustrates the
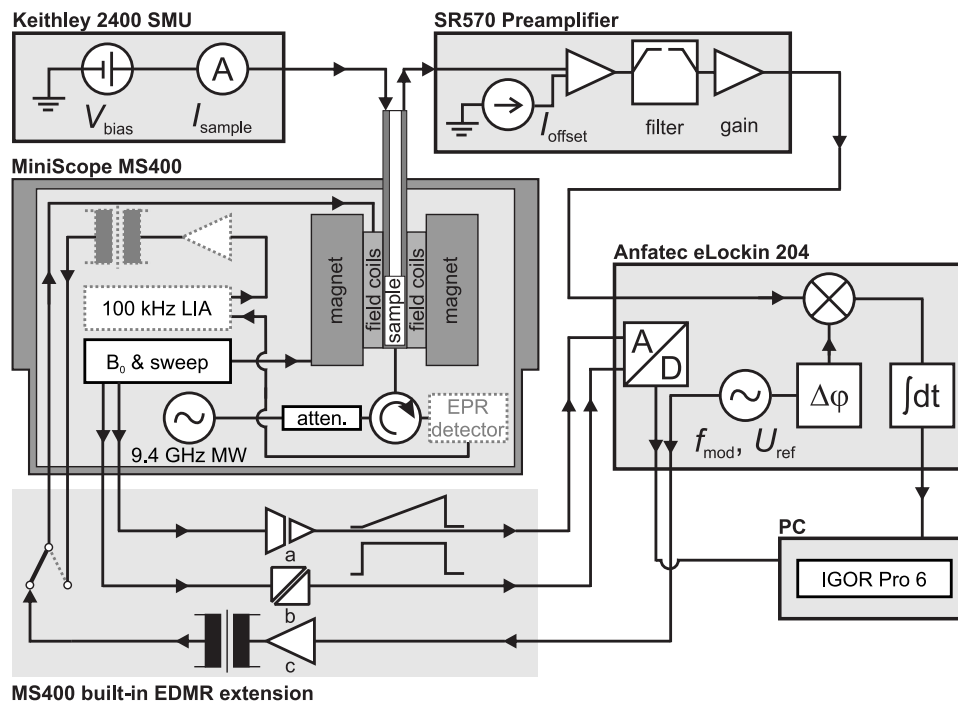

FIG. 1. Detection scheme and extensions for the EDMR setup. The sample is located inside the EPR resonance cavity and connected to a Keithley 2400 source measure unit (SMU) and a SR570 low-noise current preamplifier. The sample bias voltage V_{bias} is applied using the Keithley SMU which also measures the sample current I_{sample}. The SR570 current preamplifier is able to compensate for the sample's direct current via the offset current I_{offset}. Additionally, the SR570 offers several low-pass, high-pass and band-pass filters. Its variable gain can be set from 1 V/mA to 1 V/pA. The setup can operate in EPR or EDMR mode using either an internal fixed-frequency lock-in amplifier (LIA) at 100 kHz, the corresponding modulation amplifier and the microwave detector (dotted components), or the EDMR extension components, respectively. The newly modified B-field sweep generator creates a signal for the magnetic sweep ramp and a trigger signal. These signals are passed to the analog-to-digital converter of the lock-in amplifier (Anfatec eLockIn 204) via an isolation amplifier (a) and an optocoupler (b), respectively. In EDMR mode, the eLockIn reference sine generator output is used to drive the custom EDMR modulation amplifier (c) setting the desired modulation amplitude via the applied reference voltage amplitude U_{ref} at the chosen modulation frequency f_{mod}. All components are controlled via IGOR Pro 6, which also collects the x- and y-channel data, as well as the magnetic sweep ramp and the trigger signal from the eLockIn. Here, $\Delta\varphi$ is the phase shifter and $\int dt$ symbolizes the time integration.

EDMR detection scheme as well as the necessary extensions used in our setup. In addition to a conventional (benchtop) EPR spectrometer one needs several new components, which we describe in the following. For EDMR measurements, a stable and precise bias voltage V_{bias} has to be applied to the sample or device under test. To further investigate the sample by measuring its I/V characteristics, it is necessary to determine the current through the sample I_{sample}. Using a Keithley 2400 source measure unit (SMU), we are able to investigate the sample's characteristics very conveniently directly inside the spectrometer. Additionally, the determination of I_{sample} during an EDMR experiment opens up the possibility to set an offset current I_{offset} at the low-noise current preamplifier SR570 (Stanford Research) to compensate for the sample bias current, thus enabling sensitivity levels down to 1 pA/V. Furthermore, the SR570 preamplifier provides the ability to filter the input signal if desired, choosing from several different low-pass, high-pass and band-pass filters. As in conventional EPR spectroscopy, a signal modulation principle is beneficial to detect the rather small part of the total signal that is actually spin-dependent. In the EPR mode of the MS400 spectrometer, a fixed modulation frequency of 100 kHz is used for phase-sensitive detection. However, a lower modulation frequency is required for EDMR. Furthermore, both theory and experiment have shown a modulation frequency dependence for EDMR experiments.[8,9] It is therefore desirable to be able to freely select the modulation frequency over a wide range. For this purpose, an additional modulation amplifier for the frequency range 20 Hz – 20 kHz with suitable transformer, as well as a relay to switch between the EDMR and EPR mode, were installed inside the MS400. Instead of the 100 kHz lock-in amplifier used in the EPR mode, an external dual phase lock-in amplifier with integrated reference signal generator covering the frequency range 20 Hz – 20 kHz is used in EDMR mode. Its reference output is used to drive the EDMR modulation amplifier setting the desired modulation amplitude B_{mod} via the amplitude of the applied reference voltage U_{ref} at the chosen modulation frequency f_{mod}. For synchronizing the EDMR measurement and detection, the generation of an analogue magnetic sweep ramp output as well as a trigger signal was implemented in the B_0 & sweep generator of the MS400. To enhance signal quality, the magnetic sweep ramp and the trigger signal are galvanically isolated via an isolation amplifier and an optocoupler, respectively. Both signals are fed into the analog-to-digital converter of the Anfatec eLockIn 204 and read out synchronously with the lock-in channel data containing the EDMR signal. Using the virtual instrument software architecture (VISA protocol) to address all setup components and the powerful and extensible scientific analysis capabilities of IGOR Pro 6 (WaveMetrics, Inc.) we implemented a highly customizable and freely accessible software interface for our EDMR setup, enabling all components to work seamlessly together, e.g., providing the ability to script-control a series of measurements.

Because our benchtop setup allows for EPR as well as EDMR measurements, it is useful to briefly summarize the commons and differences of both detection modes with respect to the signal generation at this point. Figure 2 shows a comparison between the signal generation in EPR (S_{EPR}) and EDMR (S_{EDMR}) mode. While the parameters for the magnetic field ramp $B_0(t)$ (with sweep width B_{sweep} and scan time t_{scan}), as well as the microwaves U_{MW} (with amplitude U_0 adjustable by means of the attenuator) remain unchanged in both measuring modes, the applied gain T and field modulation B_{mod} do not. Here, a key point is the different signal gain, which is applied post-quadrature as a linear gain in case of EPR but pre-quadrature by the current preamplifier in the EDMR mode. Beside the different gains, a sample bias voltage V_{bias} and corresponding bias current I_{sample} are present in EDMR mode as new parameters (cf. figure 1). However, the most important aspect is the difference in the field modulation B_{mod}. For EPR there is only one modulation frequency (100 kHz) available in the MS400 tabletop spectrometer. The modulation system is resonantly tuned and optimized for that frequency, resulting in possible field modulation amplitudes of 5 μT to 0.7 mT. In contrast, the modulation frequency can be freely selected between 20 Hz and 20 kHz in the EDMR mode. Thus, the obtainable field modulation amplitude is a function of the modulation frequency f_{mod} and the applied reference voltage amplitude U_{ref}. To be able to select the desired field modulation amplitude in an EDMR experiment the modulation frequency dependency $G(f_{mod})$ has to be determined as described in the following section.

EPR mode signal S_{EPR}:

$$S_{\text{EPR}}(B_0, U_{\text{MW}}, B_{\text{mod}}^{\text{EPR}}) \times T_{\text{EPR}}$$

where $T_{\text{EPR}} = \textbf{post}\text{-quadrature gain}$

$$B_{\text{EPR}}(t) = B_0(t) + B_{\text{mod}}^{\text{EPR}} \cos(\omega_{\text{mod}}^{\text{EPR}} t)$$

where $\omega_{\text{mod}}^{\text{EPR}} = 2\pi \times 100 \text{ kHz} = \text{const.}$
and $B_{\text{mod}}^{\text{EPR}} = 5 \text{ μT} - 0.7 \text{ mT}$

EDMR mode signal S_{EDMR}:

$$S_{\text{EDMR}}(B_0, U_{\text{MW}}, B_{\text{mod}}^{\text{EDMR}}, I_{\text{sample}}) \times T_{\text{EDMR}}$$

where $T_{\text{EDMR}} = \textbf{pre}\text{-quadrature gain and } I_{\text{sample}}(V_{\text{bias}})$

$$B_{\text{EDMR}}(t) = B_0(t) + B_{\text{mod}}^{\text{EDMR}} \cos(\omega_{\text{mod}}^{\text{EDMR}} t)$$

where $\omega_{\text{mod}}^{\text{EDMR}} = 2\pi \times f_{\text{mod}} = \text{variable}$
and $B_{\text{mod}}^{\text{EDMR}} = G(f_{\text{mod}}) U_{\text{ref}}$

Parameters valid in both modes:

$$B_0(t) = B_0 - \frac{1}{2} B_{\text{sweep}} + B_{\text{sweep}} \frac{t}{t_{\text{scan}}} \qquad U_{\text{MW}}(t) = U_0 \cos(\omega_{\text{MW}} t)$$
$$\text{with } \omega_{\text{MW}} = 2\pi \times 9.4 \text{ GHz}$$

FIG. 2. Comparison between EPR and EDMR mode signal generation. The parameters are chosen in analogy to figure 1. Note the difference in gain T, as well as in the modulation amplitude B_{mod} for the different modes. The magnetic field B_0, as well as the microwave radiation U_{MW} are equal in both modes. For EDMR the relation $G(f_{\text{mod}})$ has to be investigated experimentally to determine the modulation amplitude. See text for details.

III. CHARACTERIZATION AND CALIBRATION OF THE FIELD MODULATION AMPLITUDE

As described in section II (see figure 2) the field modulation amplitude B_{mod} for the EDMR mode depends on the applied modulation voltage amplitude U_{ref} and the transfer characteristics of the used modulation transformer expressed as $G(f_{\text{mod}})$. To characterize the modulation path for the EDMR mode, the maximum possible modulation voltage amplitude $U_{\text{ref,max}}$ for the modulation amplifier as well as the resulting current through the modulation rods as a function of f_{mod} were measured carefully. Moreover, the field modulation amplitude B_{mod} was determined using a Hall effect magnetometer in AC mode, precisely positioned at the sample location in the resonance cavity at different modulation frequencies f_{mod} for an applied modulation voltage amplitude U_{ref} of 1 V. Since the resulting magnetic field strength is directly proportional to the current flowing through the modulation rods, it was possible to determine the maximum modulation amplitude $B_{\text{mod,max}}$ as a function of the modulation frequency f_{mod}. Figure 3 shows the results of this characterization. As expected, the achievable field amplitude depends on frequency. A modulation amplitude of $B_{\text{mod}} > 0.25 \text{ mT}$ can be applied to the EDMR sample over the whole frequency range. For modulation frequencies between 400 Hz and 18 kHz the maximum field modulation amplitude lies above 0.9 mT. The B-field sweep generator of the MS400 was recalibrated in EPR mode using a certified manganese standard ($^{55}\text{Mn}^{2+}$ in ZnS, Magnettech GmbH, Berlin, Germany) after implementing the
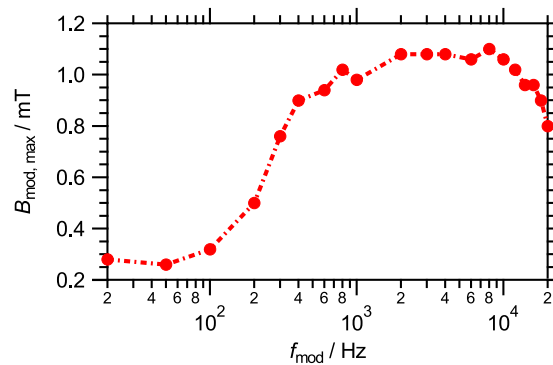

FIG. 3. Characterization of $G(f_{\text{mod}})$ for the EDMR modulation path. The maximum field modulation amplitude $B_{\text{mod,max}}$ was determined as a function of the applied modulation frequency f_{mod} ranging from 20 Hz to 20 kHz.

EDMR modifications. As a result, all spectral parameters of the standard were found to be within the specified uncertainties, including line-width, hyperfine splitting, and g-factor.

IV. EDMR SPECTRUM OF A SILICON SOLAR CELL

To characterize and validate the new benchtop EDMR setup, we made use of a μc-Si:H pin solar cell with known spectroscopic properties and reasonable EDMR signal at room temperature even without illumination.[10,11] For an overview of spin-dependent processes in microcrystalline silicon, see Stutzmann *et al.*[1]

The μc-Si:H layers were prepared by plasma enhanced chemical vapor deposition using optimized standard deposition conditions.[12] Similar solar cells comprising hydrogenated amorphous silicon and μc-Si:H were previously studied by EDMR spectroscopy, and the spectroscopic properties of the current-influencing paramagnetic centers are known to a large extent.[10,11,13] Figure 4 illustrates the basic principle of a spin-dependent recombination process via a dangling-bond defect state in such a semiconductor device. An excess electron that may get captured by a conduction band tail state takes part in the formation of a spin pair with an electron occupying an energetically lower lying dangling-bond defect state. This spin-pair formation can be described using the model introduced by Kaplan, Solomon and Mott.[14] Although it would be energetically favorable for both electrons to occupy the lower lying state, this is allowed only if both spins are antiparallel according to the Pauli exclusion principle. Therefore, altering the relative spin orientation of the spin pair by driving an EPR transition on either of the two constituents produces a singlet spin-pair state and thus allows for the initially forbidden transition to take place. The resulting charge accumulation at the dangling-bond state then attracts a hole from the valence band and eventually results in charge carrier recombination. This recombination process macroscopically influences the sample conductivity and thus alters the spin-dependent current, which is the observable in an EDMR experiment. Besides spin-dependent recombination, other spin-dependent transitions can take place depending on the material under investigation as well as on the experimental conditions. More comprehensive explanations of spin-dependent processes can be found elsewhere.[1,13–17]

A. EDMR characteristics

First, we checked the dependence of the signal area on microwave power and modulation field amplitude B_{mod}. As shown in figure 5(a), the signal area is strictly proportional to the square root
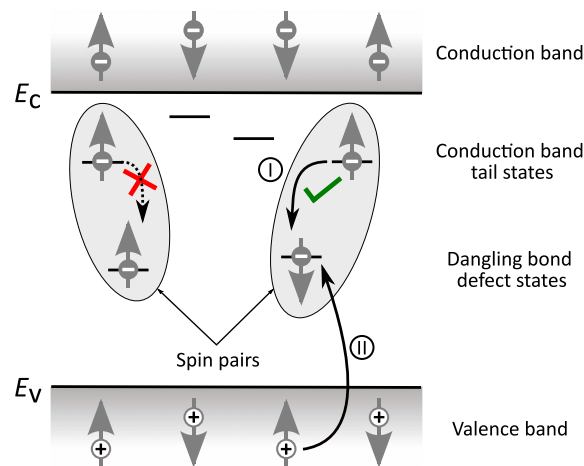

FIG. 4. Schematic representation of a spin-dependent recombination process via a dangling-bond defect state in a semiconductor device. Excess electrons may be captured by conduction band tail states from where they can move further into energetically lower lying dangling bond states only if this process is allowed for the formed spin pair according to the Pauli exclusion principle. Changing the relative spin orientation via EPR results in the transformation of a triplet (left) into a singlet pair (right) leading to charge accumulation at the dangling bond state. This charge then attracts a hole from the valence band in the second step and eventually undergoes charge carrier recombination.
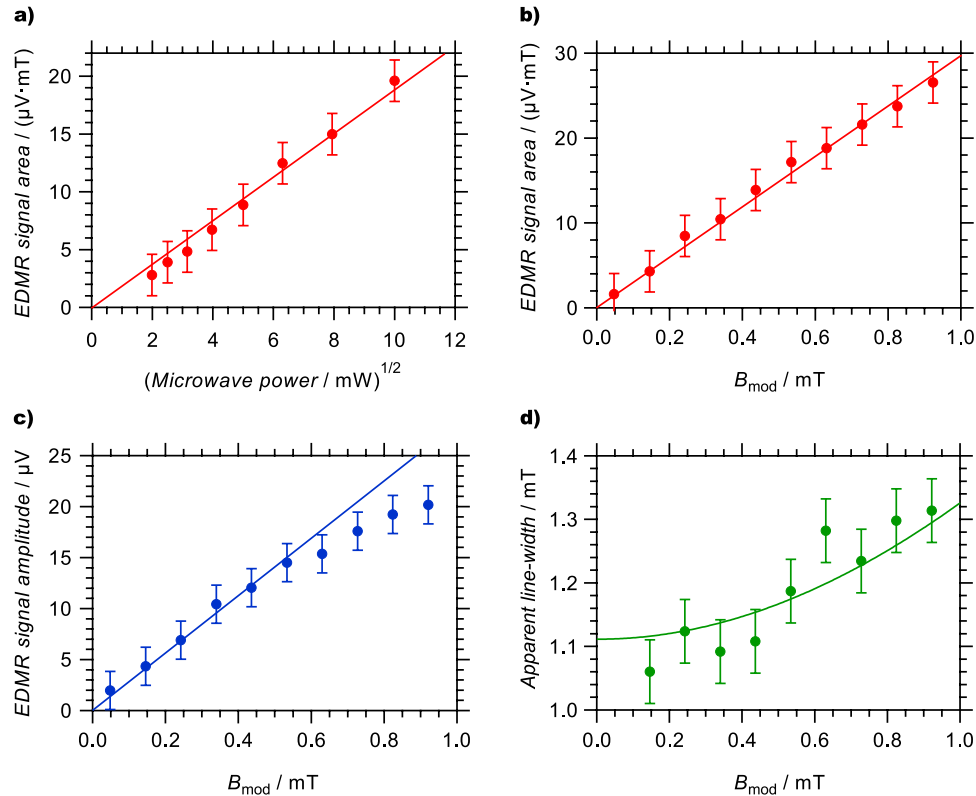
FIG. 5. EDMR characteristics of the investigated μc-Si:H type thin-film solar cell. a–b) Dependence of the EDMR signal area on (a) the applied microwave power and (b) the modulation field amplitude B_{mod}. c–d) Dependence of (c) the signal amplitude and (d) the apparent line-width ΔB_{obs} on B_{mod}. ΔB_{obs} was fitted using Poole's equation[18] for a modulation-broadened line-width, $\Delta B_{obs} = \sqrt{4\Delta B_{int}^2 + B_{mod}^2} - \Delta B_{int}$, yielding an intrinsic line-width of $\Delta B_{int} = 1.11(5)$ mT.

of the microwave power up to $P_{MW} = 100$ mW, implying that no saturation of the spin system occurs. This is to be expected in case of charge carrier recombination as the main spin-dependent process since here, the carrier pairs (and hence their spins) are destroyed by recombination in the measurement process.

Secondly, while the signal area is linear in B_{mod} over the whole experimental range (see figure 5(b)) the signal amplitude shown in figure 5(c) is linear only up to about $B_{mod} = 0.5$ mT, and then becomes sub-linear. At the same time, the apparent line-width increases from about 1.1 mT to 1.3 mT (see figure 5(d)), which is in accordance with modulation broadening, given our B_{mod} calibration (cf. section III) and an intrinsic inhomogeneous line-width of 1.11(5) mT. This value is reasonable for dangling bond states in microcrystalline silicon, for which the reported g-factors are in the range of 2.004 – 2.006 depending on the deposition conditions.[19–21] The g-factors observed here are also within this range (see section IV B). Finally, within the experimental accuracy given by the manganese standard (see section III), the g-factor does not depend at all on bias conditions or other experimental parameters, which is consistent with a single spin-dependent process prevailing in this sample.

In summary, we can attribute the EDMR signal in μc-Si:H at room temperature without illumination to spin-dependent recombination of injected charge carriers via silicon dangling bonds.

B. Quantitative comparison with a "large" spectrometer

We now compare spectra acquired both with the new setup and using a state-of-the-art "large scale" EDMR spectrometer (lab-built transient X/Q-band setup based on Bruker components). Figure 6 presents results obtained for the same sample measured in both setups, which is very
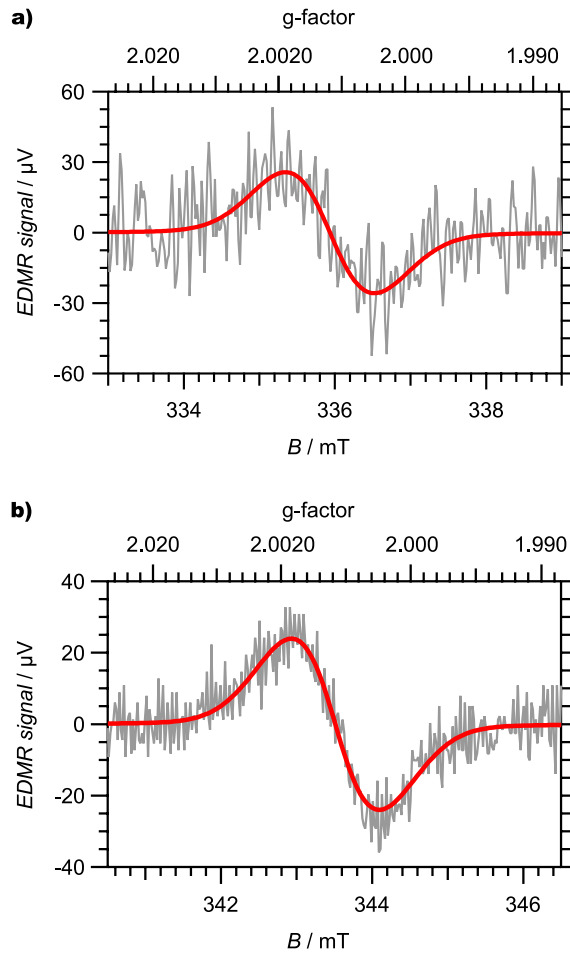
FIG. 6. EDMR spectra of the same μc-Si:H solar cell measured in (a) the new benchtop EDMR setup introduced in this article and (b) a state-of-the-art "large-scale" EDMR setup. The data were acquired at identical forward bias conditions $V_{bias} = +320$ mV. All scan parameters, including equivalent noise bandwidth of the lock-in amplifier and scan time, were chosen as similar as technically possible. The modulation frequency was set to 9876 Hz. The experimental data were fitted using a pseudo-Voigt profile.

similar in characteristics to the one investigated in figure 5. The experimental data were fitted using a pseudo-Voigt profile. For the benchtop spectrometer, a g-factor of 2.0059(3) was observed and the peak-to-peak line-width was determined to be 1.18(5) mT. For the "large" spectrometer, a g-factor of 2.0058(3) was obtained while the signal had a peak-to-peak line-width of 1.15(5) mT. Therefore, both results are equal within the experimental errors, demonstrating the correct operation of the new setup.

Furthermore, the observed signal magnitudes are comparable under nominally identical conditions. In particular, the spectrum in figure 6(a) was recorded using five times the microwave source power compared to the one shown in figure 6(b). However, the resonant cavities have different fill factor, quality factor Q, geometry, and hence different conversion factor $c = B_1 / \sqrt{P_{MW}}$. For the rectangular TE_{102} resonator of the benchtop machine, we found that the quality factor of the empty cavity, $Q \approx 6000$, decreases by about 10% upon introduction of the sample. We roughly estimate the conversion factor to be $c \approx 0.20$ mT/$\sqrt{W}$ ($\pm 10\%$) for the MS400. The dielectric ring resonator ER 4118 X-MD-5 of the "large" setup is specified as TE_{011}, $Q \approx 4000$ and $c = 0.42$ mT/$\sqrt{W}$ by the manufacturer (Bruker Corporation). Thus, the effective magnetic field strength of the microwave, B_1, is estimated to be less than 10% larger in figure 6(a) than in figure 6(b). All scan parameters (including the equivalent noise bandwidth of the lock-in amplifier and the scan time) were chosen

as similar as technically possible on both spectrometers. The spectra were acquired in reverse bias conditions using a modulation frequency of $f_{mod} = 9876$ Hz and a field modulation amplitude $B_{mod} = 0.5$ mT in both cases. Hence, the obtained signal magnitude should be comparable, which is in good accordance with the experimental results shown in figure 6.

In summary, it can be stated that the spectroscopic parameters of the used μc-Si:H solar cell could be successfully determined using the benchtop EDMR and that the signal strength is very similar.

C. Signal-to-Noise Ratio

As shown in the preceding sections, the signal is directly proportional to both, the effective microwave amplitude B_1 and the modulation amplitude B_{mod} over a wide range of parameters. Within this range, we find no discernible dependence of the g-factor and line-width, and also almost constant noise.

A comparison of the noise levels in figure 6(a) and 6(b) shows that our new setup exhibits somewhat higher noise. We have thus carried out a careful experimental noise analysis and optimization with the somewhat surprising result that the detected EDMR signal in the new setup is limited by noise generated within the sample. Extrinsic noise sources such as the used amplifiers and the bias source can be disregarded. There is a finite, if small, coupling to environmental "lab noise" due to imperfections in the cable shielding used for contacting the sample. Due to the lock-in detection employed in EDMR, this noise is however efficiently filtered out by setting a small enough equivalent noise bandwidth (ENBW, inversely related to the lock-in time constant). Furthermore, the Anfatec lock-in amplifier used here allows measuring the noise spectrum over arbitrary frequency intervals so that one can conveniently choose a modulation frequency at which the lab noise is minimized.

The modulation frequency and the electrical bias conditions, however, show a great impact on the signal-to-noise ratio. This is to be expected when considering a sufficiently detailed semiconductor model, which is however outside the scope of this paper. Even in the simplest case, where only one spin-dependent transport channel like recombination contributes to the spin-dependent EDMR current ΔI_{EDMR}, it is still in competition with all spin-independent transport mechanisms that contribute to the total current I_{sample}. Hence, for rectifying devices like diodes and solar cells, it may be advantageous to measure under reverse-bias conditions where the unwanted, spin-independent, current is small. To illustrate this effect, we show in figure 7 an EDMR spectrum of the same μc-Si:H sample as investigated in figure 6(a), but under reverse bias. The modulation

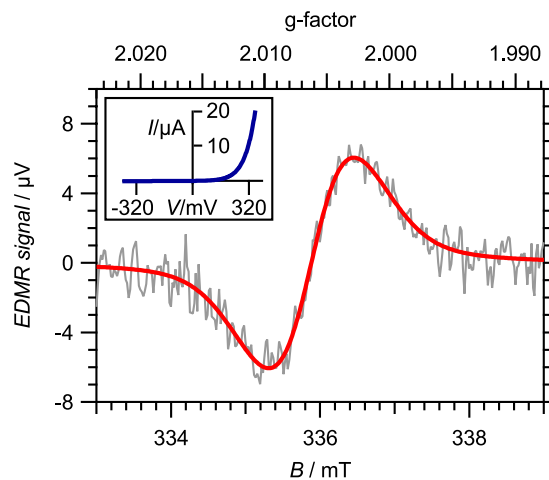FIG. 7. EDMR spectrum of the same sample as shown in figure 6(a), but under reverse bias $V_{bias} = -320$ mV and at $f_{mod} = 625$ Hz. All other parameters remained unchanged. The data were fitted using a pseudo-Voigt profile ($g = 2.0062(3)$, $\Delta B_{obs} = 1.14(5)$ mT). The inset shows the I/V characteristic of the sample.

TABLE I. Summary of the obtained results for the µc-Si:H solar cell used in figures 6(a) and 7. The preamplifier gain was set to 1 V/µA, the modulation amplitude was $B_{mod} = 0.5$ mT and the microwave source power was set to 100 mW. ΔI_{EDMR} is the peak-to-peak value of the pseudo-Voigt profile. The noise current I_{noise} was determined as the full-width at half height of a gaussian fit to a histogram of the pseudo-Voigt fit residuum. SNR is the signal-to-noise ratio.

Figure	f_{mod}/ Hz	V_{bias}/ V	I_{sample}/µA	ΔI_{EDMR}/pA	I_{noise}/pA	$\Delta I_{EDMR}/I_{sample}$	$|I_{noise}/I_{sample}|$	SNR
6(a)	9876	+0.32	13.0	51.5	30.7	4.0×10^{-6}	2.4×10^{-6}	1.7
7	625	−0.32	−0.112	−12.1	2.05	1.1×10^{-4}	1.8×10^{-5}	5.9

frequency was changed to $f_{mod} = 625$ Hz. All other parameters including the equivalent noise bandwidth of the lock-in amplifier as well as the scan time remained unchanged. Table I gives a summary of the obtained results from both measurements.

We note that the bias current I_{sample} is two orders of magnitude lower (and opposite in polarity) for the measurement shown in figure 7. At the same time, the peak-to-peak value of the spin-dependent current, ΔI_{EDMR}, has decreased only by a factor of 4.3, and the noise reduction is about a factor of 15, leading to an enhanced signal-to-noise ratio of SNR = 5.9 in figure 7 as compared to SNR = 1.7 in figure 6(a). The noise is thus strictly proportional neither to the total bias current nor to the EDMR signal, suggesting that other noise sources may be present.

To summarize, the detected noise level may vary by as much as a factor of 15 depending on biasing conditions and modulation frequency. Looking at figures 6 and 7, it is interesting to note that the modulation frequency dependence of the signal-to-noise ratio is different when measuring the same sample in both EDMR setups, even when using nominally similar biasing conditions. Since the sample and the manner of contacting it were the same in both cases, we can exclude sample-related parasitic capacitances etc. We also took care not to introduce artificial damping factors due to filters in the amplifier chain and chose settings as similar as technically possible. Due to technical reasons, we however could not ascertain the total bias current value in the "large" setup with the same accuracy as in our benchtop measurements. It may well have been smaller in figure 6(b) than the value $I_{sample} = 13$ µA in figure 6(a), which could account for some of the additional noise.

A significant difference in the EDMR setups used here remains the resonance cavity, regarding both signal strength (i.e. B_1) and excess noise introduced by the electrical field component of the microwaves (i.e. E_1). It was recently shown that rectification effects of E_1 in silicon devices can dominate the noise measured in EDMR.[6] For both aspects, the dielectric ring resonator offers more favorable characteristics due to the higher field separation and concentration. At present, this translates to a somewhat larger noise floor for the benchtop spectrometer, which is however difficult to quantify due to the complicated bias dependency. Our example shows that for each EMDR setup, choosing the optimum bias point and modulation frequency may lead to gains in SNR that are potentially large and similar to the difference between the two spectrometers.

V. APPLICATION TO ORGANIC SEMICONDUCTORS

Organic semiconductors and electronic devices, such as organic solar cells and light emitting diodes, are known to be extremely sensitive to moisture and oxygen, especially under illumination.[22,23] To prevent degradation, the characterization of such devices, e.g. their current-voltage characteristics, device efficiency etc., is thus usually carried out inside the protective environment of a glove box where the sample is also prepared. Alternatively, the devices have to be encapsulated to prevent degradation, which can be cumbersome in the case of EDMR since the whole device has to fit inside an EPR resonator. Furthermore, the encapsulation process itself may lead to unwanted chemical changes of the device due to interdiffusion of solvents or direct chemical reactions with the encapsulating agent. Nevertheless, almost all of the EDMR results on organic devices published so far have been obtained on encapsulated samples.

Being very compact, the setup presented here can be operated in a protective atmosphere, which obviates the need for device encapsulation. This not only simplifies the experimental protocol, it also makes a study of impacts of the encapsulation procedure possible. Because the additional equipment needed for EDMR was partly implemented directly into the spectrometer case itself, our setup does not extend its original footprint of $(55 \times 29 \times 40)$ cm^3. This opens up the possibility of directly handling atmosphere-sensitive types of samples in an EDMR setup for the first time.

As an example of such a type of material we investigated the EDMR spectra of crystalline fullerene microwires within the new spectrometer. Because of its delicate nature, this kind of fullerene modification has not yet been investigated in EDMR to our knowledge. Here, the close proximity between the sample preparation equipment and the applied characterization techniques, offered by the new setup, is crucial to obtain reproducible results.

We prepared wire-like crystals from a 3 mM solution of sublimed C_{60} (purity > 99.9%, confirmed by HPLC analysis) in *m*-xylene by controlled solvent evaporation.[24] The obtained microwires were then transferred onto a custom-designed EDMR substrate, which is a glass plate with interdigitated gold electrodes (spacing 10 μm, thickness 130 nm).

Besides the study of processes in dark EDMR, the presented setup is also well suited for experiments under illumination. The MS400 spectrometer has an additional port that can be used to introduce a light fiber bundle ending right at the optimal sample position inside the resonance cavity. This fiber optic allows for the selection of a proper light source for the experiment or device under test. In this study we used a KL 2500 LCD halogen cold light source (Schott, Germany) set to a total luminous flux at the light guide exit of $\Phi_V = 500$ lm. Figure 8(a) illustrates the used coplanar EDMR sample structure and shows a typical C_{60} wire of several microns in length that was transferred to the coplanar gold structure. Figure 8(b) depicts the corresponding current-voltage characteristics of this sample under illumination. Here, the expected non-ohmic behavior of C_{60} as an organic semiconductor is observed, showing the successful transfer on and connection to the gold electrode structure. The investigated sample consisted of only very few of these fullerene wires, still giving a measurable current signal.

Figure 9 shows a light-induced EDMR spectrum obtained from a fullerene-microwire sample similar to the one shown in figure 8. The observed EDMR signal corresponds to a small change in conductivity of $\Delta\sigma/\sigma = \Delta I_{\mathrm{EDMR}}/I_{\mathrm{Sample}} \approx 8 \times 10^{-5}$, which is comparable to that of thin-film devices.[25,26] The corresponding g-factor was determined to be 2.0022(3), which is in accordance with a value observed earlier in C_{60} thin-film devices studied by p-EDMR.[25] In cw-EDMR, signals at $g = 2.0017 - 2.0020$ were reported and attributed to spin-dependent recombination of
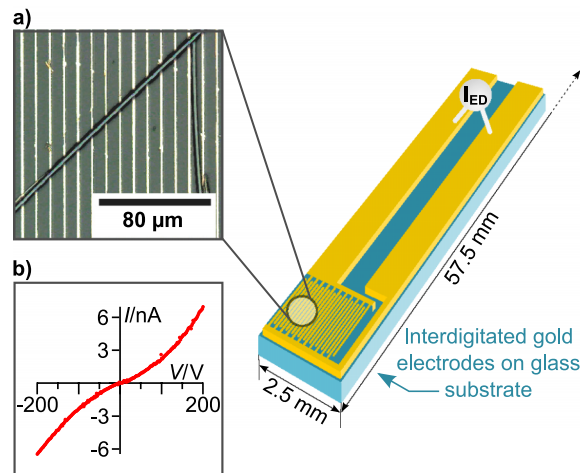

FIG. 8. Illustration of the used EDMR sample structure and (a) laser scanning microscope picture (Keyence VK-8710K) of the transferred fullerene microwires on coplanar gold electrodes (spacing 10 μm, thickness 130 nm), (b) corresponding I/V characteristic recorded inside the EDMR spectrometer using a KL 2500 LCD halogen cold light source (luminous flux at the light guide exit $\Phi_V = 500$ lm).
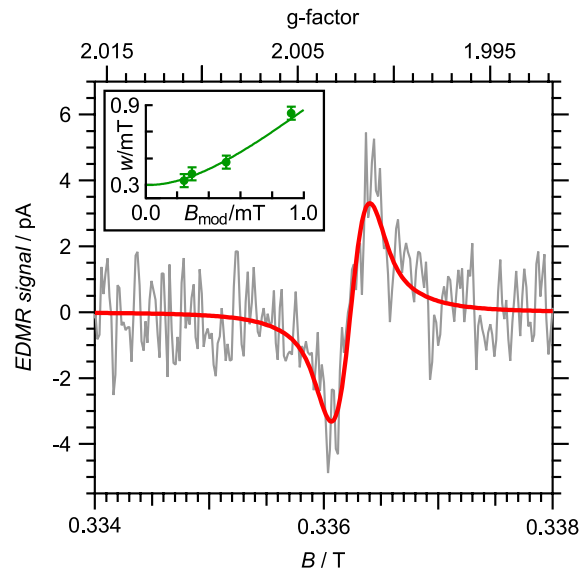
FIG. 9. Light-induced EDMR spectrum of C_{60} microwires crystallized from 3 mM *m*-xylene solution. The data were acquired at $V_{bias} = -150$ V and $f_{mod} = 625$ Hz. The experimental data were fitted using a pseudo-Voigt profile, resulting in $g = 2.0022(3)$ and $\Delta B_{obs} = 0.33(5)$ mT. The inset shows the apparent line-width w at different B_{mod} settings. Using a fit similar to figure 5(d), the intrinsic line-width was found to be $\Delta B_{int} = 0.30(5)$ mT.

photo-generated, non-geminate charge carrier pairs presuming either a polaron pair as the precursor for the recombination or a defect site formed by impurities.[17,26,27] However, as discussed earlier,[2,25] we attribute the observed EDMR signal to spin-dependent recombination of charge carriers at photo-generated fullerene dimer impurities such as C_{120} or $C_{120}O$. The slightly higher g-factor observed here may be due to the fact that our fullerene wires can be presumed to be much more crystalline,[24,28] than any of the thin films investigated earlier.[25] Accordingly, the transport states are more delocalized and may form band tails, resulting in a g-factor increased towards the free electron value $g = 2.0023$.

As depicted in the inset of figure 9, we could determine the intrinsic inhomogeneous line-width of the signal to be $\Delta B_{int} = 0.30(5)$ mT by varying the used modulation field amplitude (B_{mod}) and fitting the data with the equation for the observed modulation broadened line-width ΔB_{obs}.[18] Again, this is in excellent agreement with our earlier investigations in thin-film samples of C_{60}.[25]

Summarizing the very first results on fullerene microcrystals obtained in this study, one can conclude that the investigation of semiconductor crystals is now possible using the EDMR method. This type of study can lead to a gain in sensitivity of the method because of the possible scale-down of the number of charge carriers involved in the EDMR experiment. Minimizing the investigated crystals, and therefore optimizing the device structures to restrict the current flow to a narrow region, one can engineer the device's EDMR characteristics and gain new insights in the processes involved in charge carrier mobility, recombination and so forth. Furthermore, a large family of organometallic molecules, which is too atmosphere-sensitive to handle outside of a glove box, can now be investigated by means of EDMR. The application of the introduced compact EDMR is not limited to organic semiconductors and organometallics in glove box environments, but can also be extended to other constricted environments, like clean rooms inside semiconductor device facilities.

VI. CONCLUDING REMARKS

In summary, we built a compact setup for measuring electrically detected magnetic resonance of semiconductor devices that yields consistent and highly reproducible results. Using a standard silicon solar cell for a detailed comparison with a typical "large-scale" setup, we could show that the EDMR spectra are quantitatively comparable in all spectroscopic dimensions with those obtained

in a state-of-the-art spectrometer. As an application example highlighting the benefits of close proximity between device fabrication and spectroscopic characterization possible with the compact setup introduced here, we recorded EDMR spectra of organic C_{60} microwires, a class of samples never before investigated in EDMR.

As shown, the presented setup allows the study of processes in dark EDMR and under illumination. Furthermore, the stabilization of the sample temperature as well as measurements at low or elevated temperatures are possible using the available temperature-controlling unit for the spectrometer. Thus, the presented setup can be used for complete semiconductor device characterization at different operating conditions.

Due to its small footprint, the unit is highly mobile and can in particular be operated inside cleanrooms or even glove boxes, which is beneficial for studies on organic materials and devices such as the fullerene microwires shown here, as well as for other atmosphere-sensitive materials.

Routine investigations can easily be realized with this instrument, enabling more research groups interested in magnetic resonance phenomena to get started with EDMR. Finally, although the EPR spectrometer itself is compact and closed, the electrical detection pathway is entirely accessible to the researcher in order to study recently discussed phenomena like the dependence of the signal phase of EDMR signals on modulation frequency.[8]

[1] M. Stutzmann, M. S. Brandt, and M. W. Bayerl, J. Non. Cryst. Solids **266-269**, 1 (2000).

[2] W. Harneit, C. Boehme, S. Schäfer, K. Huebener, K. Fostiropoulos, and K. Lips, Phys. Rev. Lett. **98**, 216601 (2007).

[3] J. Behrends, A. Schnegg, K. Lips, E. A. Thomsen, A. K. Pandey, I. D. W. Samuel, and D. J. Keeble, Phys. Rev. Lett. **105**, 176601 (2010).

[4] T. Herring, S.-Y. Lee, D. McCamey, P. Taylor, K. Lips, J. Hu, F. Zhu, A. Madan, and C. Boehme, Phys. Rev. B **79**, 195205 (2009).

[5] D. R. McCamey, K. J. van Schooten, W. J. Baker, S.-Y. Lee, S.-Y. Paik, J. M. Lupton, and C. Boehme, Phys. Rev. Lett. **104**, 017601 (2010).

[6] C. C. Lo, F. R. Bradbury, A. M. Tyryshkin, C. D. Weis, J. Bokor, T. Schenkel, and S. A. Lyon, Appl. Phys. Lett. **100**, 063510 (2012).

[7] J. A. Weil and J. R. Bolton, *Electron Paramagnetic Resonance: Elementary Theory and Practical Applications*, 2nd ed. (John Wiley & Sons, Hoboken, NJ, 2006).

[8] S.-Y. Lee, S. Paik, D. R. McCamey, and C. Boehme, Phys. Rev. B **86**, 115204 (2012).

[9] C. Yang, E. Ehrenfreund, F. Wang, T. Drori, and Z. Vardeny, Phys. Rev. B **78**, 205312 (2008).

[10] C. Meier, J. Behrends, C. Teutloff, O. Astakhov, A. Schnegg, K. Lips, and R. Bittl, J. Magn. Reson. **234**, 1 (2013).

[11] J. Behrends, A. Schnegg, C. Boehme, S. Haas, H. Stiebig, F. Finger, B. Rech, and K. Lips, J. Non. Cryst. Solids **354**, 2411 (2008).

[12] W. Böttler, V. Smirnov, J. Hüpkes, and F. Finger, Phys. Status Solidi A **209**, 1144 (2012).

[13] A. Schnegg, J. Behrends, M. Fehr, and K. Lips, Phys. Chem. Chem. Phys. **14**, 14418 (2012).

[14] D. Kaplan, I. Solomon, and N. Mott, J. Phys. Lettres **39**, 51 (1978).

[15] D. Lepine, Phys. Rev. B **6**, 436 (1972).

[16] F. Rong, W. Buchwald, E. Poindexter, W. Warren, and D. J. Keeble, Solid. State. Electron. **34**, 835 (1991).

[17] T. Eickelkamp, S. Roth, and M. Mehring, Mol. Phys. **95**, 967 (1998).

[18] C. P. Poole, *Electron Spin Resonance: A Comprehensive Treatise on Experimental Techniques* (Interscience Publishers, New York, 1967), p. 400.

[19] P. Kanschat, K. Lips, and W. Fuhs, J. Non. Cryst. Solids **266-269**, 524 (2000).

[20] O. Astakhov, R. Carius, Y. Petrusenko, V. Borysenko, D. Barankov, and F. Finger, Phys. Stat. Sol. (RRL) **1**, R77 (2007).

[21] F. Finger, L. B. Neto, R. Carius, T. Dylla, and S. Klein, Phys. Status Solidi C **1**, 1248 (2004).

[22] P. E. Burrows, V. Bulovic, S. R. Forrest, L. S. Sapochak, D. M. McCarty, and M. E. Thompson, Appl. Phys. Lett. **65**, 2922 (1994).

[23] N. Grossiord, J. M. Kroon, R. Andriessen, and P. W. Blom, Org. Electron. **13**, 432 (2012).

[24] L. Wang, B. Liu, D. Liu, M. Yao, Y. Hou, S. Yu, T. Cui, D. Li, G. Zou, A. Iwasiewicz, and B. Sundqvist, Adv. Mater. **18**, 1883 (2006).

[25] S. Schäfer, K. Hübener, W. Harneit, C. Boehme, K. Fostiropoulos, H. Angermann, J. Rappich, J. Behrends, and K. Lips, Solid State Sci. **10**, 1314 (2008).

[26] I. Hiromitsu, Y. Kaimori, M. Kitano, and T. Ito, Phys. Rev. B **59**, 2151 (1999).

[27] M. S. Brandt, "Spinabhängiger Transport und Rekombination in Halbleitern," Phd thesis (in german) (University of Stuttgart, 1992).

[28] T. Wakahara, T. Kato, K. Miyazawa, and W. Harneit, Carbon **50**, 1709 (2012).